

Parameter Determination and Drive Control Analysis of Axial Flux Permanent Magnet Synchronous Motors

Attila Nyitrai^{1*}, Gergely Szabó², Sándor R. Horváth²

¹ Multidisciplinary Doctoral School of Engineering Sciences, Széchenyi István University, H-9026 Győr, Egyetem tér 1., Hungary

² Department of Electric Power Engineering, Faculty of Electrical Engineering and Informatics, Budapest University of Technology and Economics, H-1111 Budapest, Egrý József street 18., Hungary

* Corresponding author, e-mail: nyitrai.attila@sze.hu

Received: 16 December 2021, Accepted: 11 March 2022, Published online: 31 March 2022

Abstract

Axial flux electric motors have received a lot of attention in recent years due to successful implementations in industrial or traction applications. Particularly, axial flux permanent magnet synchronous motors (AFPMSM) can be an attractive choice in case of high torque-density requirements or when the drive environment (packaging) is geometrically limited to a disc-shaped motor. However, compared to radial flux motors, axial flux machine modeling possibilities are much less documented. In the present study, different electromagnetic modeling approaches have been compared through an example AFPMSM design. The motor parameters were determined by analytical and finite element methods. A 2D equivalent model (2D Linear Motor Modeling Approach – 2D-LMMA) and a 3D model results have been compared. The calculated values were used to carry out a drive control analysis of the axial flux motor.

Keywords

axial flux motor, motor parameters, drive control simulation, electromagnetic analysis, finite element analysis

1 Introduction

Axial flux (AF) permanent magnet synchronous motors (AFPMSM) have some particular advantages when compared to radial flux (RF) counterparts. An obvious advantage compared to RF motors is the usually higher specific torque when using simple cooling arrangements [1, 2]. The electromagnetic torque of the axial flux motor is proportional to the third power of the outer diameter of the active parts [3]:

$$T_{EM,AF} \propto D_o^3. \quad (1)$$

In case of radial flux motors, the output electromagnetic torque is proportional to the rotor volume (a classical sizing method of RF motors is based on the torque per rotor volume (TRV) value):

$$T_{EM,RF} \propto D_{ro}^2 L, \quad (2)$$

where D_{ro} is the rotor outer diameter and L is the working active length of the machine. From the above equations it can be seen, that the axial and radial flux motors have different proportions (L/D); AF motors are less suitable for smaller power applications especially when the outer diameter is limited by packaging constraints of the

environment. On the other hand, the output power of the AF motor increases more significantly with the diameter when the active length has less influence on the performance [3]. Applications, where high specific power (torque) is necessary is therefore the area where AF motors can demonstrate comparative advantage to RF motors.

Generally, in order to evaluate and compare the motor characteristics of different designs in real-world working conditions, the modeling of the different physical phenomena in electric machines is necessary. Recently, multiphysics analysis has been in the focus of many researchers, where the advantages of such modeling approaches were presented. In [4] particularly, a multiphysics modeling approach through the design of a permanent magnet assisted synchronous reluctance motor (PMSynRM) were presented. It was shown, that the importance of multiphysics analysis in order to optimize high specific power machines is vital. The multiphysics model of the electric machine addresses at least the following physical phenomena:

- Electromagnetic Analysis;
- Thermal Analysis;
- Mechanical Analysis;

- Structural (Strength Analysis);
- Rotordynamic Analysis;
- Drive Control Analysis;
- NVH Analysis.

In Sections 2 and 3, as part of a multiphysics motor model of the axial flux machine, an electromagnetic and drive control analysis with parameter determination is presented. In Section 1, the importance of axial flux motors and their research are presented. The reason for parameter estimation of electric motors is discussed. The different approaches of parameter estimation are briefly described. In Section 2, the electromagnetic modeling methods of axial flux motors are presented. In addition to a simple analytical model, 2D and 3D finite element models are presented. The parameters of a given example AF motor are calculated using the different approaches and compared in Subsection 2.4. Based on the calculated parameters, the drive control analysis of the motor is presented in Section 3. The 2D and 3D analysis was prepared using FEMM and Maxwell software respectively. The drive control analysis was carried out using Matlab/Simulink software.

1.1 Parameter estimation

The motor parameters can be used in numerical simulations by applying system models in order to determine the dynamic behavior of the motor during real load-cycle conditions. In case of traction motors, it is important to evaluate the motor performance during standardized drive-cycles in order to prove that the machine will meet the specifications of electromagnetic and thermal performance. Usually, due to the computationally expensive finite element model, it is not possible to directly couple electromagnetic and thermal field solvers with the other components of the system model, such as the drive and control model. This is especially the case in early design iterations. Therefore, reduced order models are applied in order to evaluate the models in a reasonable time. In order to define the basic parameters of the motor, generally, the magnetic circuit model of the motor needs to be evaluated. The motors' parameters can be used for further analytical investigations in order to find working point parameters and therefore to quickly evaluate the performance of the machine and drive.

In case of permanent magnet synchronous motors (PMSM), we can basically group the machines to motors with magnetically isotropic and anisotropic rotors. Latter machines with rotor saliency can be either classified as

interior permanent magnet (IPM) or permanent magnet assisted synchronous reluctance machines (PMSynRM). This category of motors has a significant reluctance torque component in their electromagnetic torque. From the motor parameters' point of view, these motors are generally more complicated, since the two main inductance parameters L_d and L_q are different. In addition, magnetic saturation affects the two inductance components differently. In many cases, due to the nonlinear behavior of the magnetic model of these machines, it is more convenient to prepare a parameter sweep through the corresponding I_d and I_q values and determine the flux-linkages directly. These flux-linkage tables (maps) parameterized with I_d and I_q can be directly used during numerical simulations. However, the drawback of this method is that compared to the motor parameter approach, the nonlinear behavior of the machine is rather hidden from the designer.

2 Electromagnetic modeling of axial flux motors

AFPMSMs are known to be three-dimensional structures regarding their electromagnetic properties. The disc-shaped airgap has a flux-density distribution that is not only varies by the angle around the axis of rotation, but it is a function of the radial dimension as well. Therefore, several modeling approaches were introduced [5–7] to prepare low or high-fidelity electromagnetic models of AF machines suitable for different calculations such as sizing, analytical evaluation of the magnetic circuit. Generally, lower fidelity 2D FEA-based methods are used to evaluate nonlinear effects and naturally the highest fidelity models can be built by applying the finite element method on 3D geometries. In [8], the authors presented a dynamic model of an AFPMSM made from soft magnetic composite core material. The authors used magnetic equivalent circuits to analyze the quasi-static electromagnetic behavior. In [9], the authors described a both steady-state and transient finite element modeling of axial flux permanent magnet motors and compared the results with measurements. An analytical non-linear magnetic circuit modeling approach was presented in [10], where the authors validated the model results with 3D-FEA. In [11], the authors presented a quasi-3D magnetic equivalent circuit modeling approach and validated the model by measurements.

2.1 Analytical methods

The traditional approach to determine electric motor working point properties is the analytical electromagnetic modeling using the lumped parameter (lumped circuit)

modeling method (LPM or LCM). In this case, a magnetic equivalent circuit model of the machines is built in order to determine the main magnetic flux components in the motor and therefore through the magnetic flux-linkages, calculate the inductance values. In the present study, an analytical approach described in [3] was implemented.

The PM flux:

$$\Phi_{PM} = \frac{\alpha B_{pk} (R_o^2 - R_i^2) \pi}{p} \quad (3)$$

where α is the ratio of average to peak flux densities:

$$\alpha = \frac{B_{avg}}{B_{pk}} \quad (4)$$

The armature fluxes in the d- and q-axes respectively:

$$\Phi_{ad,q} = \frac{2}{\pi} B_{pkad,q1} \frac{\pi R_o^2 - R_i^2}{p} \quad (5)$$

From the fluxes and number of turns, the flux-linkages in the d- and q-axes can be determined respectively.

The d- and q-axis flux-linkages therefore:

$$\Psi_{d,q} = \frac{1}{\sqrt{2}} N_1 k_{w1} \Phi_{ad,q} \quad (6)$$

The d- and q-axis inductances are therefore can be calculated by the expression:

$$L_{ad,q} = \frac{\Psi_{ad,q}}{I_{ad,q}} = m \mu_0 \frac{1}{\pi} \left(\frac{N_1 k_{w1}}{p} \right)^2 \frac{(R_o^2 - R_i^2)}{g_{d,q}} k_{fd,q} \quad (7)$$

The equation of the electromagnetic torque:

$$T_{EM} = \frac{3}{2} \cdot p \cdot [\lambda_m \cdot i_q + (L_d - L_q) \cdot i_d \cdot i_q], \quad (8)$$

where T_{EM} is the electromagnetic torque, λ_m is the permanent magnet flux-linkage, L_d, L_q are the d- and q-axis inductances and i_d, i_q are the d- and q-axis currents respectively.

Equations (3)–(8) have been applied using the main parameters and geometry of the motor (Fig. 1 and Table 1). The results are presented and compared to the other methods in Subsections 2.3 and 2.4. The analytical approach considers an even distribution of the airgap flux-density along the radial dimension of the airgap.

2.2 2D finite element methods

Generally, the possible 2D modeling approaches for dual-rotor axial-flux motors are 2D-LMMA (Linear Motor Modeling Approach), 2D-IRMA (Internal Rotor Modeling Approach) and 2D-ORMA (Outer Rotor Modeling

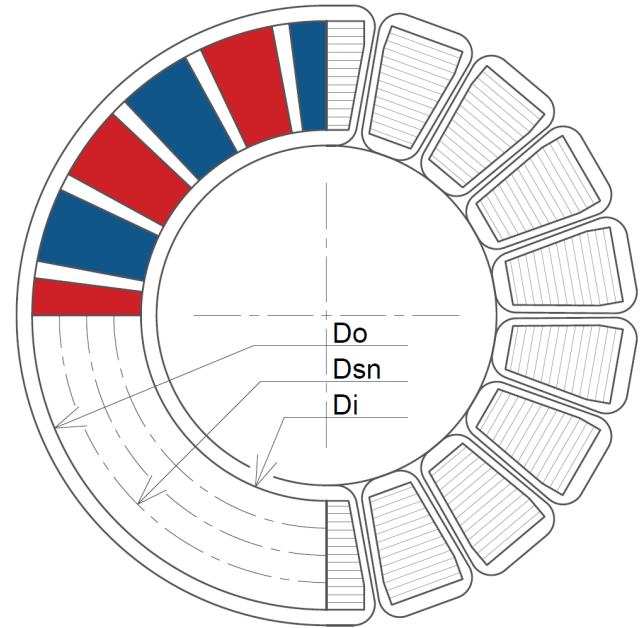


Fig. 1 Geometrical arrangement of the active components of an axial flux motor. D_o is the outer diameter, D_i is the inner diameter, D_{sn} is the diameter of the n^{th} 2D segment used in the equivalent model.

Table 1 Main parameters of the calculated motor.

Parameter	Value	Dimension
DC Voltage	670	[VDC]
Max. Current	250	[ARMS]
Number of Poles	20	[-]
Stator outer diameter (SOD)	200	[mm]
Stator inner diameter (SID)	130	[mm]
Rotor outer diameter (ROD)	200	[mm]
Rotor inner diameter (RID)	130	[mm]
Magnet thickness	6	[mm]
Airgap length	0.8	[mm]

Approach) as presented in [5]. Using the multi-slice method, or the 2D-LMMA, the axial flux motor can be modeled in two dimensions; since the magnetic flux-density distribution varies in the radial direction, depending on the particular design, a set of 2D equivalents, or "slices" can be introduced to estimate the whole motor's magnetic properties with less error [12]. However, the same method can be applied by directly solving the Maxwell-equations on simple geometries as presented by [6]. The disadvantage of the latter method is that it is less generally applicable on different geometries than the finite element method.

The analysis steps of the 2D equivalent finite element modeling of the AF motor are the followings:

1. Determine the model symmetries in the direction of rotation based on the number of slots (N_s) and number of poles ($2P$);

2. Determine the number of slices and prepare the 2D geometric representations of the motors;
3. Application of the electromagnetic boundary conditions of the Linear Motor Modeling Approach as presented in Fig. 2;
4. Definition of the magnetic material properties;
5. Application of the electromagnetic excitations;
6. Meshing and mesh sensitivity analysis;
7. Solution of the 2D finite element models;
8. Evaluation of the results.

The results of the 2D FEA are presented in Fig. 3 and Fig. 4. In Fig. 3, the magnetic flux density plot is presented. In Fig. 4, the flux-linkages of the different sections can be observed.

2.3 3D finite element methods

Compared to the 2D approach using the multi-slice method, the 3D finite element method ensures a proper modeling of a set of three-dimensional effects including the radial air-gap flux density distribution of AF motors. Obviously, 3D electromagnetic modeling is a straightforward approach

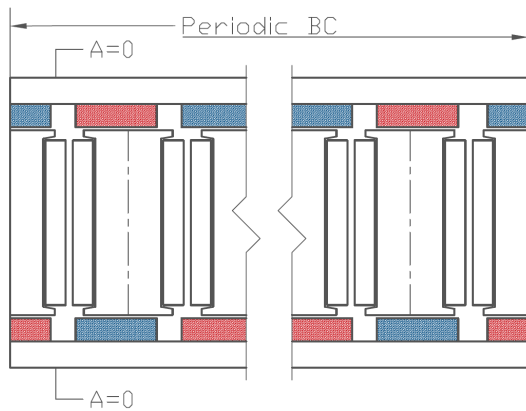


Fig. 2 A slice of the 2D equivalent model of the motor. On the model boundaries periodic and $A=0$ boundary conditions should be applied.

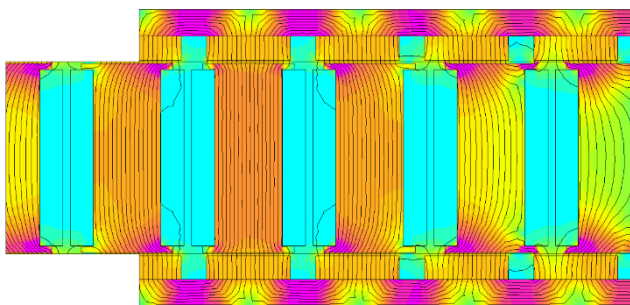


Fig. 3 Magnetic flux density plot and flux lines of the equivalent 2D model in open-circuit condition.

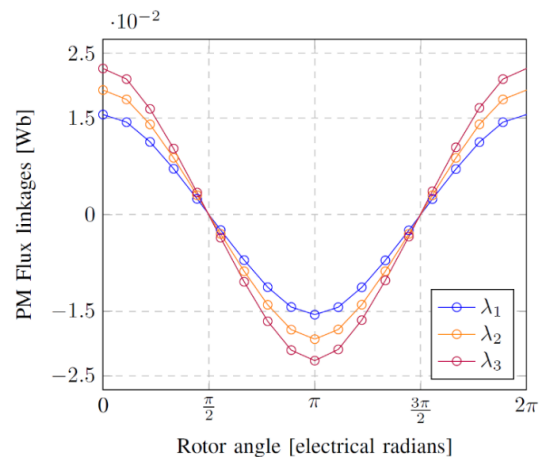


Fig. 4 Permanent magnet flux linkages of the different slices of the 2D equivalent model. Slice 1: λ_1 , slice 2: λ_2 slice 3: λ_3

for modeling anisotropic, three-dimensional structures without an easy-to-prove 2D equivalent, such as in the case of axial flux machines.

An additional benefit of using 3D analysis is the possibility for proper consideration of end-effects, offering more precise calculation of e.g. end-winding leakage and related stray losses in structural parts. Such end-effects are to be investigated dominantly in radial direction regarding dual rotor, sandwich-like axial flux topologies.

2.3.1 Yokeless and segmented stator modeling

Generally, in terms of rotating electric machines, a yoke is considered as a material of high magnetic permeability for providing a flux path between adjacent poles.

Considering technological possibilities of winding-automation, the stator core should be segmented to obtain a feasible geometry for mass production. Such yokeless stator structure can be observed in Fig. 5, where each coil is to be wound around an individual segment.

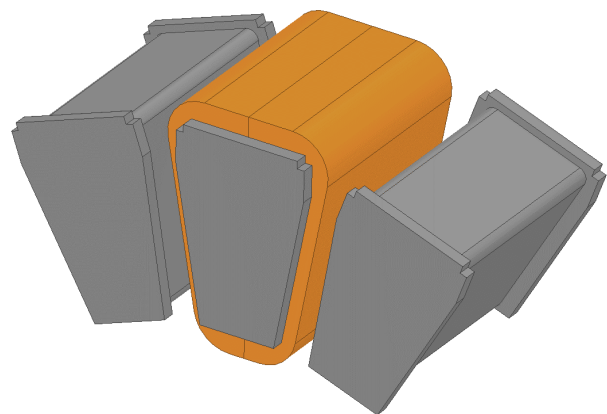


Fig. 5 Yokeless and segmented stator design with simplified winding geometry, prepared for 3D electromagnetic analysis.

The main advantages of applying this yokeless stator design are related to mass reduction, (increased specific power [kW/kg]) and efficiency improvement due to lower total core loss gained by the elimination of hysteresis loss.

2.3.2 Rotating band setup

In order to model the relative displacement between stationary and rotating parts, most software require a special region, usually called band, to be defined at the centerline of airgap. In case of an axial-flux PMSM with dual rotor topology, as illustrated by Fig. 6, the practical approach is to define a single band in such a way that it encloses all the stator core segments and windings. By applying a rotating band, the need for complete remeshing at every time step can be avoided, leading to a significant reduction of simulation time and computational resources.

2.3.3 Mesh generation

Discretization of the 3D model space is carried out using tetrahedron elements. During a transient solution process, adaptive mesh generation (typical e.g. in case of eddy-current problems) is not possible, so the relevant set of Maxwell's equations are evaluated for the same nodes at every time step. Proposed initial mesh density for rough 3D transient analysis is presented in Fig. 7.

In volumes where the intensity of magnetic field is high, usually around the air gap and end-winding area of a rotating machine, mesh quality holds key importance for simulation fidelity and time demand of calculations.

The mesh type and the number of the elements is indicated in Table 2 in case of 2D and 3D FEA, corresponding to the precision level of presented results.

2.3.4 Simulation of no-load characteristics

The peak value of the flux-linkage is 0.064 [Vs] using the selected magnet grade *N35H* ($H_c = -840$ [kA/m], $\mu_r = 1.06$)

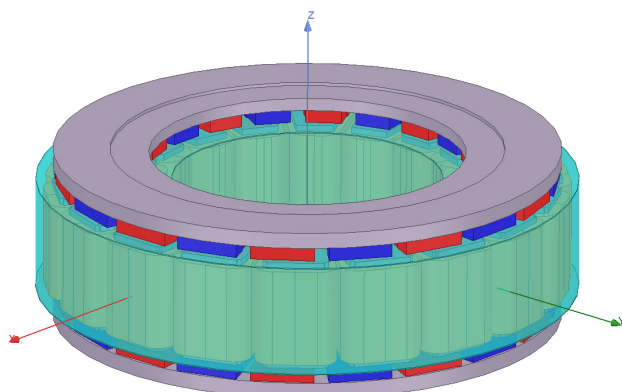


Fig. 6 3D model and rotating band setup of the yokeless axial flux permanent magnet motor topology.

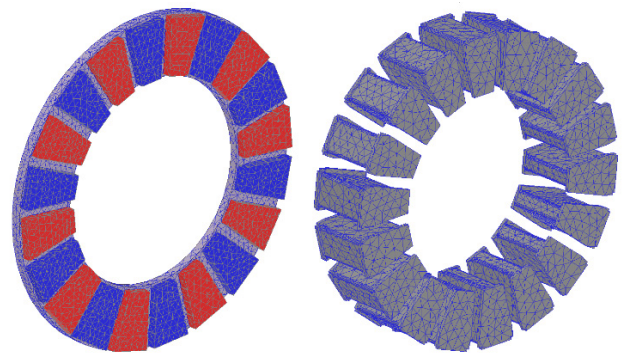


Fig. 7 Mesh of the 3D model. The rotor and stator represented separately.

Table 2 Comparison of the mesh properties.

Variable name	2D FEA	3D FEA
Element type	Triangle	Tetrahedron
Number of elements	45203	243199

at 20 [°C]. The simulated no-load line-to-line voltage at each time step over a complete electrical period is presented in Fig. 8. Applying previously presented mesh density for rough transient study, the calculated average torque is practically zero, with numerical pulsation between ± 200 [mNm] region.

2.3.5 Simulation of short-circuit characteristics

Just like the similar characteristic measurement, the simulation of short-circuit condition should be performed in generator mode, forcing a constant shaft speed regardless the magnitude of electromagnetic torque and output current.

Short-circuit characteristics obtained by transient 3D simulation are presented in below Fig. 9.

According to IEEE 812-1984 standard [13], performing short-circuit measurement with a suitable external reactance (limiting the current e.g. to its rated value) is a reasonable approach to obtain steady-state temperature rise when inverter-coupled test cannot be carried out.

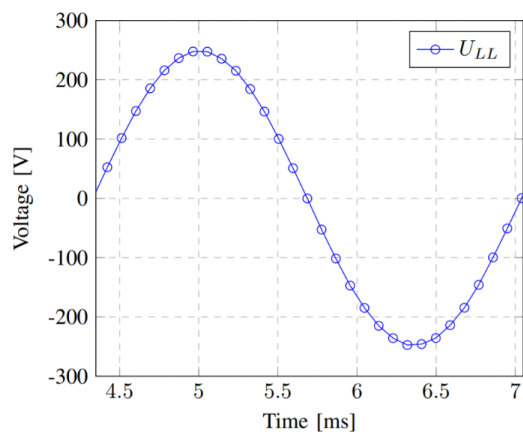


Fig. 8 No-load Line-to-Line voltage at 2200 [1/min].

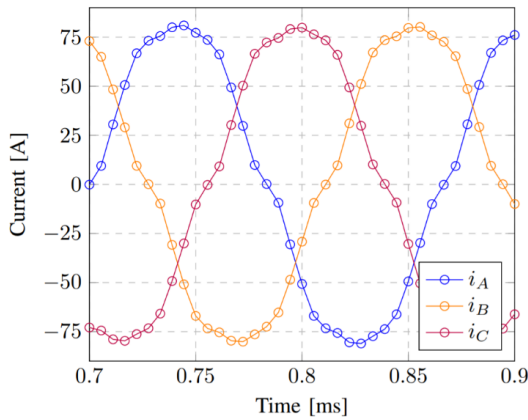


Fig. 9 Short-circuit current at 40 [1/min] speed.

2.3.6 Simulation of rated load

The electromagnetic (airgap) torque of synchronous machines is traditionally expressed as a function of load-angle δ , which is expected to be sinusoidal in case of a surface-mounted (magnetically symmetric) rotor design. Flux-density in magnetically active parts, corresponding to maximum torque operating point, is visualized by Fig. 10.

Based on identical operating conditions, the comparison of torque profiles between 3D FEA and 2D-LMMA methods can be studied in Fig. 11.

In Fig. 10 linear scale was applied between 0 [T]–2.2 [T] to visualize magnetic field. Flux-density in Permanent Magnet parts was also checked to ensure that rated operating point is feasible with reversible demagnetization.

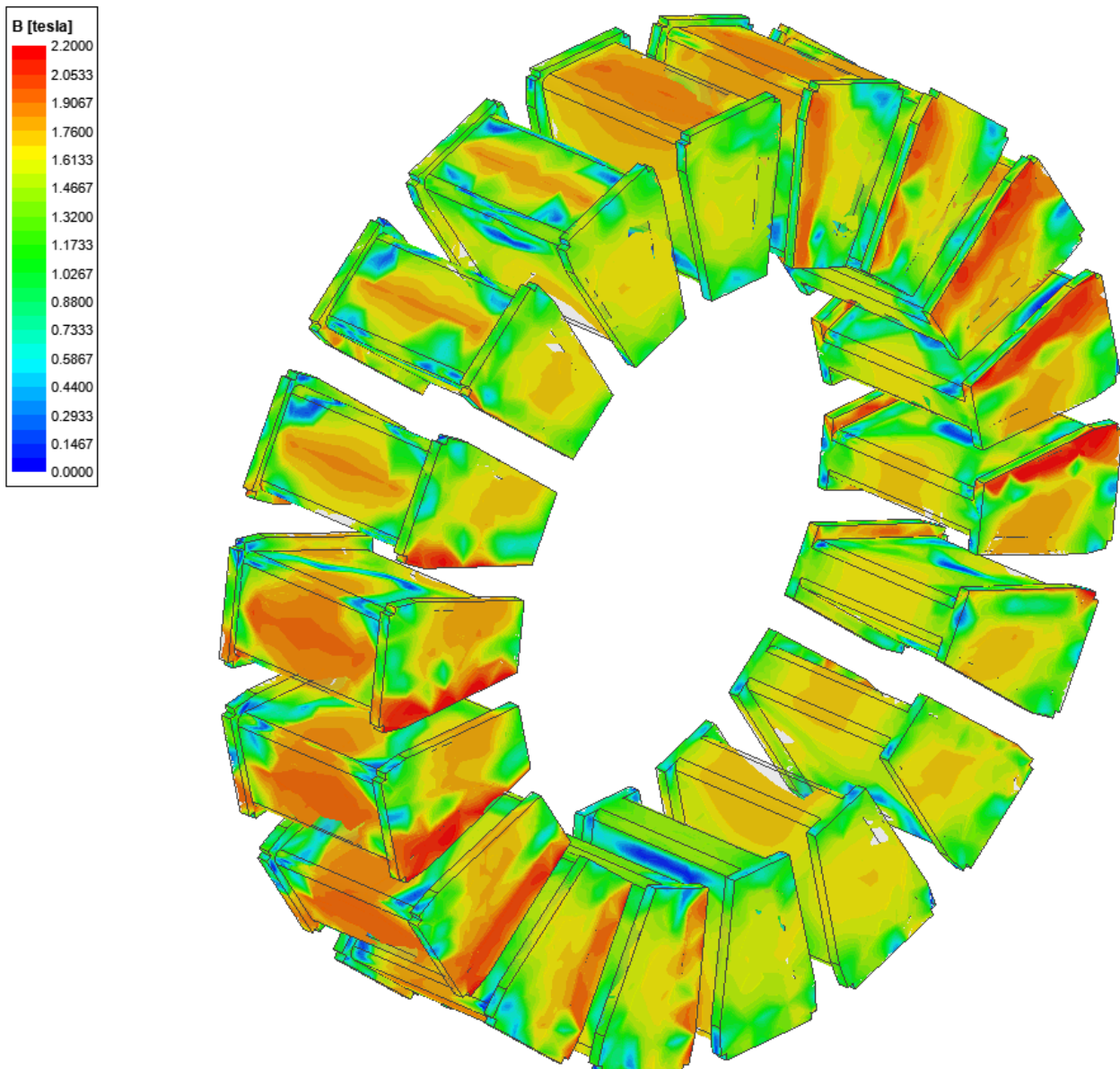


Fig. 10 Flux-density of stator segments at rated load condition.

Result for each load-angle was obtained by 3D magnetostatic simulation, using a self-developed scripting method to eliminate repetitive human procedures.

2.4 Comparison of the results of the different methods

The calculated motor parameter values have been compared. The d- and q-axis inductances and the PM flux-linkages have been compared applying the different calculation methods. From the results the following conclusions have been drawn. In case of an early design analysis, the analytical method is appropriate. On the other hand, the simple analytical calculation does not include non-linear effects, such as magnetic saturation. Regarding the FEA methods, the 2D equivalent and the 3D FEA results are suitable for the further drive control analysis, because the difference was approximately 12.5%.

It was found, that the computation time of the 3D model was significantly longer, however, the multi-slice method required more manual work to prepare the geometry of the sections. If the geometry preparation was automatized, then it can be concluded, that the 2D FEA method is preferred, in case of geometrical optimization and when more variants are also necessary to be evaluated. The authors propose a workflow where the motor parameters are calculated in the following order:

Pre-design by analytical motor parameter calculation (no saturation effects considered):

- 2D equivalent model for geometrical optimization and motor parameter determination in each step, considering non-linear effects;
- 3D FEA for the final determination of the motor parameters, considering non-linear effects on a true 3D model.

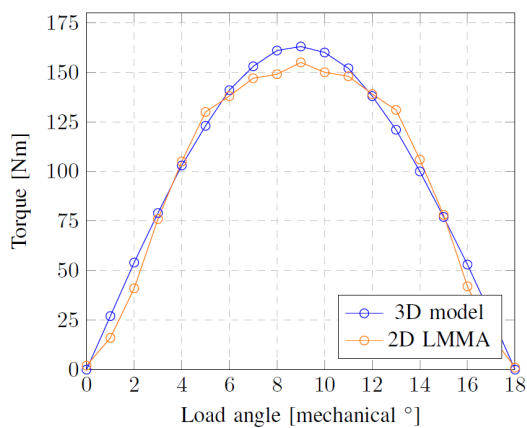


Fig. 11 Comparison of Torque characteristics using 100 [Apk] supply.

In Table 3, the motor parameters are compared. The analytical torque value calculated from Eq. (8) in case of q-axis current is 186 Nm, therefore the error compared to the result from the 3D model is 11%.

3 Drive control analysis

3.1 Dynamic concentrated parameter model

The drive control part of the analysis attempted to test the machine's behavior under controlled dynamic conditions. This approach is based on the machine's differential system of equation which is the following for the selected machine type (AFPMSM):

$$u_d = Ri_d + L_d \frac{di_d}{dt} - \omega_{\Psi_p} L_q i_q, \quad (9)$$

$$u_q = Ri_q + L_q \frac{di_q}{dt} + \omega_{\Psi_p} L_d i_d + \omega_{\Psi_p} \Psi_p, \quad (10)$$

$$m = \frac{3}{2} p ((L_d - L_q) i_d i_q + \Psi_p i_q), \quad (11)$$

$$J \frac{d\omega}{dt} = m - m_l - F\omega, \quad (12)$$

where u_d, u_q are the real and imaginary parts of the stator voltage vector, i_d, i_q are the real and imaginary parts of the stator current vector respectively, F is the friction loss factor, J is the moment of inertia, ω is shaft angular speed.

The presented machine model points out that an axial flux, permanent magnet machine's model does not differ from the radial one's.

The machine model was parameterized using the primary magnetostatic FEM simulations, where inductance and flux parameters were calculated. This also defines an improvement option [14], which can provide significantly better, but yet computationally not too expensive machine model, and its steps can be summarized as follows:

- calculating the flux profiles of the machines in direct and quadratic direction using predefined current combinations. By doing this the inductance profiles of the machine can be calculated and its integration into the machine model results in saturating behavior,

Table 3 Comparison of the results.

Variable name	Analytical	2D FEA	3D FEA
d-axis inductance (L_d), [μH]	218	204	208
q-axis inductance (L_q), [μH]	207	203	197
PM flux-linkage (Ψ_{PM}), [Wb.turns]	0.062	0.056	0.064

- calculating cogging torque profile of the machine. This can be modelled as the difference of machine model's torque and FEM calculated torque.

The developed control structure was the widely used PI cascade control loop as shown in Fig. 12, where every C denotes a controller and their subscripts indicate their purpose.

To achieve better utilization of the machine MTPA algorithm was implemented [15], which provided current reference for both current controllers. The PI-type controllers were modelled as follows:

$$G_{PI}(s) = A_p \left(1 + \frac{1}{sT_i} \right), \tag{13}$$

where A_p is the proportional gain, T_i is the integral time. The tuning was performed based on the predefined cut-off frequency and damping factor [16], which resulted the parameters in Table 4.

3.2 Simulation results

The simulation target was to verify the machine model's response during no-load and nominal load conditions. The test speed – torque covered the four quadrants.

Fig. 13 summarizes the simulation results, where the nominal speed and load was examined. Fig. 13(a) and (b) shows the d- and q-direction current components.

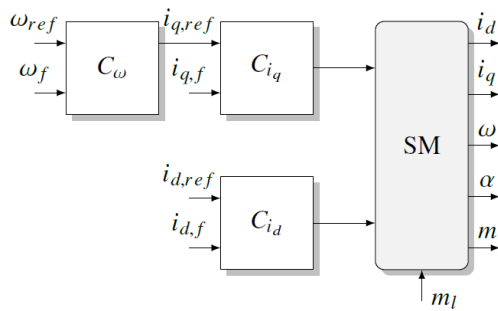


Fig. 12 Cascade control loop.

Table 4 Field oriented cascade control loop parameters.

Parameter	Value	Description
$A_{p\omega}$	2.8252	Speed controller proportional gain
$T_{i\omega}$	66.7 ms	Speed controller integral time
A_{pd}	0.2939	Direct direction current controller proportional gain
T_{id}	1.1 ms	Direct direction current controller integral time
A_{pq}	0.4385	Quadratic direction current controller proportional gain
T_{iq}	1.5 ms	Quadratic direction current controller integral time

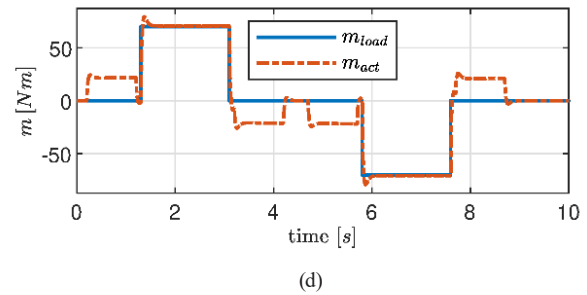
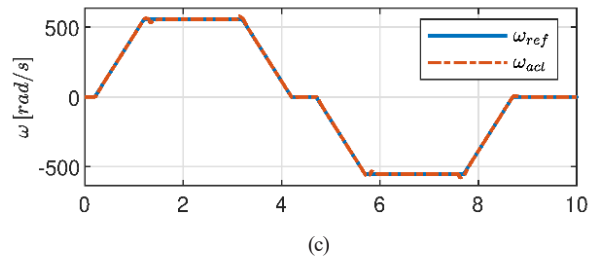
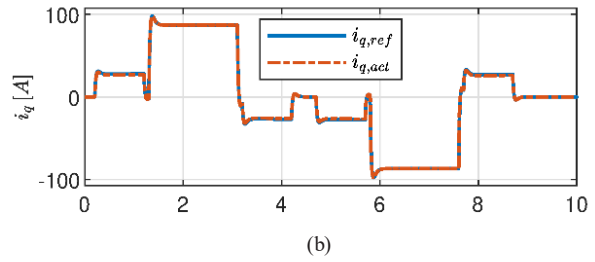
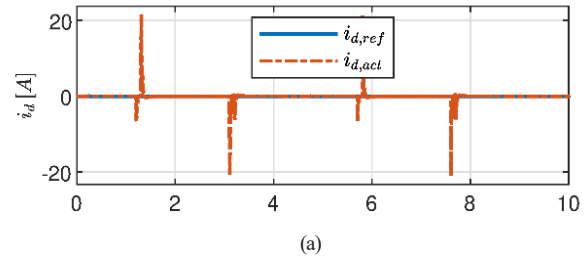


Fig. 13 Drive control analysis results; (a) d-direction current; (b) q-direction current ; (c) angular speed; (d) torque.

The first one usually tends to have nearly zero value expect the load transients. Beside the implemented MTPA the requested d-direction current is still relatively small, since the direct and quadratic inductance difference is very small. The q-direction current component correlates with the load and dynamic events, and also the current controllers were stable. Fig. 13(c) and (d) show the mechanical response of the motor. The angular speed control was stable, with good dynamics even in load drops.

3.3 The control algorithm's further possibilities

The presented control loop contains PI type controllers, but other control structures are still promising. Model Predictive Control is being published for many

applications, including field-oriented controls of rotating machines [17, 18]. Other possibilities could be the implementation of sensorless algorithms, which offers many possibilities.

One approach could be a model-based solution, for example an Extended-Kalman filter-based approach [19]. Another solution could be a non-model-based solution, such as high-frequency voltage injection methods. [20, 21].

4 Conclusion

In the present study, different methods for the determination of axial flux motor parameters have been presented. Analytical, 2D and 3D finite element methods have been compared in case of an example AFPMSM. It was found, that analytical methods for the d- and q-axis inductance calculation are suitable for the quick estimation of the motor parameters, however, in case of complicated geometries, and in order to consider non-linear behaviour, a general numerical method is more practical to use. The 2D finite element model, compared to the 3D one was found to reduce the computational time significantly, however, more manual work and more complicated model setup is necessary because of the equivalent geometries. During the drive control analysis, it was found that similar methods used in case of radial flux PMSMs were sufficient. Using the FEA calculated motor parameters the built-up drive control simulation was able to reproduce the nominal load operating of the motor, and provided stable control in the four quadrants. Authors are going to conduct further research in order to establish integrated design techniques for AFPMSM machines.

Nomenclature

AF axial flux;
AFIR axial flux internal rotor;

AFPM Axial flux permanent magnet (~motor);
BC boundary condition;
EMAG electromagnetic;
EMF electro-motive force;
FE finite element;
FEA finite element analysis;
FEM finite element modeling;
IRMA Internal Rotor Modeling Approach;
LMMA Linear Motor Modeling Approach;
MEC magnetic equivalent circuit;
PM permanent magnet;
RF radial flux;
RFPM radial flux permanent magnet (~motor);
SPM surface (-mounted) permanent magnet;
SynRM synchronous reluctance motor.

List of symbols

Φ_{PM} permanent magnet flux;
 α ratio of average and peak ;
 B_{avg} average flux-density;
 B_{pk} peak flux-density;
 R_o outer radius;
 R_i inner radius;
 $\Psi_{d,q}$ flux-linkage (d or q axis);
 N_1 number of turns per phase;
 k_{w1} winding factor (fundamental);
 $\Phi_{ad,q}$ armature flux (d or q axis);
 $L_{ad,q}$ boundary condition;
 T_{EM} electromagnetic torque;
 p number of pole pairs;
 λ_m magnet flux-linkage;
 i_q q-axis current;
 i_d d-axis current;
 L_d d-axis inductance;
 L_q q-axis inductance.

References

- [1] Patterson, D. J., Colton, J. L., Mularcik, B., Kennedy, B. J., Camilleri, S., Rohoza, R. "A comparison of radial and axial flux structures in electrical machines", In: 2009 IEEE International Electric Machines and Drives Conference, Miami, FL, USA, 2009, pp. 1029–1035.
<https://doi.org/10.1109/IEMDC.2009.5075331>
- [2] Cavagnino, A., Lazzari, M., Profumo, F., Tenconi, A. "A comparison between the axial flux and the radial flux structures for PM synchronous motors", IEEE Transactions on Industry Applications, 38(6), pp. 1517–1524, 2002.
<https://doi.org/10.1109/TIA.2002.805572>
- [3] Gieras, J. F., Wang, R. J., & Kamper, M. J. "Principles of AFPM Machines", In: Axial Flux Permanent Magnet Brushless Machines, Springer, Dordrecht, Netherlands, 2005, pp. 27–78.
https://doi.org/10.1007/1-4020-2720-6_2
- [4] Nyitrai, A., Szabó, G., Horváth, S., Vajda, I. "Multiphysics Analysis of Automotive PMaSynRM", In: 2019 International IEEE Conference and Workshop in Óbuda on Electrical and Power Engineering (CANDO-EPE), Budapest, Hungary, 2019, pp. 67–72.
<https://doi.org/10.1109/CANDO-EPE47959.2019.9111009>
- [5] Gulec, M., Aydin, M. "Implementation of different 2D finite element modelling approaches in axial flux permanent magnet disc machines", IET Electric Power Application, 12(2), pp. 195–202, 2018.
<https://doi.org/10.1049/iet-epa.2017.0434>

- [6] Tiegna, H., Bellara, A., Amara, Y., Barakat, G. "Analytical Modeling of the Open-Circuit Magnetic Field in Axial Flux Permanent-Magnet Machines with Semi-Closed Slots", *IEEE Transactions on Magnetics*, 48(3), pp. 1212–1226, 2012.
<https://doi.org/10.1109/TMAG.2011.2171979>
- [7] Egea, A., Almandoz, G., Poza, J., Ugalde, G., Escalada, A. J. "Axial-Flux-Machine Modeling With the Combination of FEM-2-D and Analytical Tools", *IEEE Transactions on Industry Applications*, 48(4), pp. 1318–1326, 2012.
<https://doi.org/10.1109/TIA.2012.2199450>
- [8] Maloberti, O., Figueredo, R., Marchand, C., Choua, Y., Condamine, D., Bommé, E. "3-D-2-D Dynamic Magnetic Modeling of an Axial Flux Permanent Magnet Motor With Soft Magnetic Composites for Hybrid Electric Vehicles", *IEEE Transactions on Magnetics*, 50(6), Article number: 8201511, 2014.
<https://doi.org/10.1109/TMAG.2014.2300152>
- [9] Hill-Cottingham, R. J., Coles, P. C., Rodger, D., Lai, H. C. "Finite element modelling of an axial flux PM machine", In: *Second International Conference on Power Electronics, Machines and Drives (PEMD 2004)*, Edinburgh, UK, 2004, pp. 552–555.
<https://doi.org/10.1049/cp:20040347>
- [10] Kano, Y., Kosaka, T., Matsui, N. "A Simple Nonlinear Magnetic Analysis for Axial-Flux Permanent-Magnet Machines", *IEEE Transactions on Industrial Electronics*, 57(6), pp. 2124–2133, 2010.
<https://doi.org/10.1109/TIE.2009.2034685>
- [11] Vansompel, H., Sergeant, P., Dupré, L. "Optimized Design Considering the Mass Influence of an Axial Flux Permanent-Magnet Synchronous Generator With Concentrated Pole Windings", *IEEE Transactions on Magnetics*, 46(12), pp. 4101–4107, 2010.
<https://doi.org/10.1109/TMAG.2010.2070075>
- [12] Nyitrai, A., Orosz, T. "FEM-Based Benchmark Problem for Cogging Torque Minimization of Axial Flux Permanent-Magnet Motors in Artap Framework", *Periodica Polytechnica Electrical Engineering and Computer Science*, 65(2), pp. 152–159, 2021.
<https://doi.org/10.3311/PPee.17755>
- [13] Institute of Electrical and Electronics Engineers "IEEE 812-1984 IEEE Standard Definitions of Terms Relating to Fiber Optics", Institute of Electrical and Electronics Engineers, Piscataway, NJ, USA, 1984.
- [14] Szabó, G., Veszprémi, K. "FEM-Parameterized Sensorless Vector Control of PMSM Using High-Frequency Voltage Injection", In: *Doctoral Conference on Computing, Electrical and Industrial Systems*, Costa de Caparica, Portugal, 2021, pp. 226–239.
https://doi.org/10.1007/978-3-030-78288-7_22
- [15] Preindl, M., Bolognani, S. "Optimal State Reference Computation With Constrained MTPA Criterion for PM Motor Drives", *IEEE Transactions on Power Electronics*, 30(8), pp. 4524–4535, 2015.
<https://doi.org/10.1109/TPEL.2014.2354299>
- [16] Wang, L., Chai, S., Yoo, D., Gan, L., Ng, K. "PID and Predictive Control of Electrical Drives and Power Converters using MATLAB/Simulink", John Wiley & Sons Inc., Singapore, Singapore, 2015.
- [17] Morel, F., Lin-Shi, X., Retif, J. M., Allard, B., Buttay, C. "A Comparative Study of Predictive Current Control Schemes for a Permanent-Magnet Synchronous Machine Drive", *IEEE Transactions on Industrial Electronics*, 56(7), pp. 2715–2728, 2009.
<https://doi.org/10.1109/TIE.2009.2018429>
- [18] Preindl, M., Bolognani, S. "Model Predictive Direct Speed Control with Finite Control Set of PMSM Drive Systems", *IEEE Transactions on Power Electronics*, 28(2), pp. 1007–1015, 2013.
<https://doi.org/10.1109/TPEL.2012.2204277>
- [19] Dilys, J., Stankevič, V., Łuksza, K. "Implementation of Extended Kalman Filter with Optimized Execution Time for Sensorless Control of a PMSM Using ARM Cortex-M3 Microcontroller", *Energies*, 14(12), Article number: 3491, 2021.
<https://doi.org/10.3390/en14123491>
- [20] Szabó, G., Veszprémi, K. "Sensorless Vector Control of Permanent Magnet Synchronous Machine Using High-Frequency Signal Injection", *Acta Polytechnica Hungarica*, 17(4), pp. 145–163, 2020.
<https://doi.org/10.12700/2FAPH.17.4.2020.4.8>
- [21] Szabó, G., Veszprémi, K. "Sensorless Vector Control of Permanent Magnet Synchronous Machine Using High-Frequency Rotating Injection", In: *2021 IEEE 19th International Power Electronics and Motion Control Conference (PEMC)*, Gliwice, Poland, 2021, pp. 588–593.
<https://doi.org/10.1109/2FPEMC48073.2021.9432563>